

# Two-component asymmetric dark matter via bound states and freeze-in decay

Mathias Becker\*

*Fakultät für Physik, TU Dortmund, D-44221 Dortmund, Germany*

Wei-Chih Huang<sup>†</sup>

*CP<sup>3</sup>-Origins, University of Southern Denmark,*

*Campusvej 55 DK-5230 Odense M, Denmark*

## Abstract

We propose a novel mechanism to realize two-component asymmetric dark matter of very different mass scales through bound state formation and late freeze-in decay. Assuming a particle-antiparticle asymmetry is initially shared by SM baryons and two dark matter components, we demonstrate that the existence of bound states formed by the heavy component can efficiently transfer the asymmetry from the heavy to the light component via late decay. In this case, the energy densities of the two components can be comparable, and the correct relic density is reproduced.

*Preprint: DO-TH 19/27    CP3-Origins-2019-43 DNR F90*

---

\*Electronic address: mathias.becker@tu-dortmund.de

<sup>†</sup>Electronic address: huang@cp3.sdu.dk

## I. INTRODUCTION

The identity of dark matter (DM), an important missing piece in the standard model (SM), remains mysterious although the astrophysical evidence of DM is well established. The DM relic density is precisely known to be  $\Omega_{\text{DM}} = 0.26$  [1, 2], inferred from the measurements of the power spectrum of the cosmic microwave background radiation. Any realistic DM model has to reproduce this value. Furthermore, possibilities that DM consists of more than one species have been studied widely; for instance, multiple light species including neutrinos and axions [3, 4] or in the context of supersymmetry involving axinos [5, 6]. Alternatively, all components can be Weakly Interacting Massive Particles (WIMPs) whose stability is protected by a discrete symmetry, parity or gauge symmetry; see, e.g., Refs. [7–21] and also Ref. [22] on the classification of two-component DM models and relic density computation.

Models of two-component DM with very different masses, featuring boosted DM [23], draw quite attention. The heavy component, that can accumulate at the galactic center or be trapped around the center of the sun, annihilates into the highly relativistic light component, which in turn can enhance the DM-nucleon interaction rate at DM detectors [23–25]. To be more specific, a relativistic DM particle can yield a large momentum transfer in DM direct detection or up-scatter into a heavier state via inelastic scattering [26] such that even DM of sub-GeV or below can be potentially probed in direct searches. That is unlike the conventional scenarios with non-relativistic DM particles where the experimental sensitivity plummets for DM lighter than a few GeV. On the other hand, the appealing idea of asymmetric dark matter (ADM) has been proposed [27] (also Refs. [28, 29] for reviews) to link the DM relic density to the baryon asymmetry, that is also unaccountable in the SM framework. In this case, either DM particles or antiparticles remain in the universe due to a local or global asymmetry, analogous to the one that distinguishes baryons from anti-baryons. In addition, generation mechanisms of baryon and DM asymmetries are often interwoven, leading to roughly comparable amounts of asymmetry in the two sectors and hence implying a DM mass of  $\sim 5$  GeV.

It is intriguing to meld these two ideas, i.e., two-component ADM of very different masses ( $\sim$  GeV and  $\gtrsim 100$  GeV respectively). A grave repercussion will be an excessive relic density, if both the light and the heavy components have roughly the same amount

of asymmetry as the SM baryons. In other words, the resulting total DM relic abundance would overclose the universe as the heavy component is by far too heavy to have a number density similar to that of the baryons. The problem can be circumvented if the asymmetry generation mechanisms for two DM species are not related or the amounts of asymmetry are controlled by independent parameters; for instance, they are generated by decays of two different heavy bosons or of the same heavy boson but with different couplings<sup>1</sup>. In this situation, the number density of the heavy component can be arbitrarily small without exceeding the observed DM density.

In this work, we explore an alternative scenario which employs bound state formation (BSF) via a long-range interaction. The interaction arises when the underlying mediator is much lighter than the interacting particles, giving rise to the so-called Sommerfeld effect (or Sommerfeld enhancement) [33, 34]. The enhancement increases the DM annihilation rate [35, 36] and opens up new regions of the parameter space, previously not viable. Besides, induced BSF among DM particles and/or heavy states can also assist depleting the relic density [37–40]. Such the long-range interactions are considered in the context of co-annihilation (with a slightly heavier but nearly degenerate partner [41, 42]) and also in supersymmetric models; see, e.g., Refs [35, 36, 39, 43–73]. Recently, it has been pointed out that the Higgs boson can induce BSF as long as it is much lighter than particles forming bound states [74, 75]. Furthermore, during the BSF process scattering with particles from the thermal bath will significantly enhance the BSF cross-section in some cases [76].

In our setup, there exist two DM sectors which separately contain the light and heavy component,  $\chi$  and  $\psi$ . We assume a particle-antiparticle symmetry was created by an unspecified mechanism at a early time and was (roughly) equally shared by  $\chi$ ,  $\psi$  and SM baryons. The realization of two-component ADM of distinctive masses relies on long-distance Yukawa interactions among particles of  $\psi$  and  $\bar{\psi}$ . The resulting  $\psi$ - $\bar{\psi}$  bound state facilitates the elimination of the symmetric component, while the remaining asymmetric component consists of bare  $\psi$  particles or bound states. As we shall see below, the ratio of the number density of the bound states to that of the bare  $\psi$  is controlled by the binding energy of the

---

<sup>1</sup> It has been demonstrated that ADM can have a very different mass from GeV in the context of two-sector leptogenesis [30, 31], where the right-handed neutrinos decay both into the SM and DM particles with dissimilar amounts of asymmetry. Models of ADM with a much heavier mass can also be realized in the context of bosonic technicolor [32].

bound state. The bound state will eventually *freeze-in* [77–79] decay to a pair of  $\chi$  (not a particle-antiparticle pair) via annihilations of the constituents of the bound state. Therefore, the final densities of  $\chi$  and  $\psi$  will depend on the aforementioned ratio between the bare  $\psi$  and the bound states before the decay. For sizable Yukawa couplings, the majority of the asymmetry of  $\psi$  will be converted into that of  $\chi$ . In the presence of a disparity in the number densities,  $n_\psi \ll n_\chi$ , the corresponding energy densities can still be of the same order,  $\Omega_\chi \sim \Omega_\psi$ , due to the distinct particle masses.

Note that this scenario is not the minimal setup to realize two-component ADM. Instead of the freeze-in mechanism, one can, for instance, have standard freeze-out of annihilations of  $\psi$  into  $\chi$  or SM fermions without involving bound states at all. The correct DM abundance can be reproduced by carefully tuning relevant coupling constants. We argue that long-range interactions (bound states) themselves have rich and profound phenomenological implications. Moreover, there could exist situations where having  $\psi$  in thermal equilibrium at early times will erase the induced asymmetry. To be more concrete, if annihilations of  $\psi$  into SM fermions ( $\psi\psi \leftrightarrow \bar{f}f$ ) and the asymmetry generation mechanism are present at the same time, there will be no initial asymmetry of  $\psi$  and thus no two-component ADM.

The paper is organized as follows. In Section II, we briefly review the formalism of Boltzmann Equations which is used to obtain the time evolution of the particle densities. Section III will be devoted to detail a simple model and the sequence of the asymmetry shift among the different particle species. Next, we show numerical results in Section IV and examine effects of several relevant parameters on the relic density. Four benchmark sets of the parameters are presented that can realize two-component ADM with comparable energy densities. Finally, we conclude in Section V. Computations of all relevant annihilation cross-sections as well as bound state formation and dissociation are collected in the Appendices.

## II. BOLTZMANN EQUATIONS

To begin, we shortly review the Boltzmann equations used to find the time evolution of the various particle densities. More detailed discussions can be found in Refs. [42, 80, 81]. Due to the expansion of the universe, a convenient quantity to describe the particle number density is  $Y \equiv n/s_{\text{en}}$ , the particle number density normalized to the entropy density  $s_{\text{en}}$ , i.e., the number of particles per comoving volume. The Boltzmann equation for the DM particle

$\chi$  reads

$$z H s_{\text{en}} \frac{dY_\chi}{dz} = - \sum_{\{a_i\}, \{f_j\}} [\chi a_1 \cdots a_n \leftrightarrow f_1 \cdots f_m], \quad (1)$$

where  $z = m_\chi/T$  and  $H$  is the Hubble parameter, while

$$\begin{aligned} [\chi a_1 \cdots a_n \leftrightarrow f_1 \cdots f_m] &= \frac{n_\chi n_{a_1} \cdots n_{a_n}}{n_\chi^{\text{eq}} n_{a_1}^{\text{eq}} \cdots n_{a_n}^{\text{eq}}} \gamma^{\text{eq}}(\chi a_1 \cdots a_n \leftrightarrow f_1 \cdots f_m) \\ &\quad - \frac{n_{f_1} \cdots n_{f_m}}{n_{f_1}^{\text{eq}} \cdots n_{f_m}^{\text{eq}}} \gamma^{\text{eq}}(f_1 \cdots f_m \leftrightarrow \chi a_1 \cdots a_n). \end{aligned} \quad (2)$$

The symbol  $\gamma^{\text{eq}}$  stands for the interaction rate in thermal equilibrium, defined as

$$\begin{aligned} \gamma^{\text{eq}}(\chi a_1 \cdots a_n \rightarrow f_1 \cdots f_m) &= \int \frac{d^3 p_\chi}{2E_\chi (2\pi)^3} e^{-\frac{E_\chi}{T}} \times \prod_{a_i} \left[ \int \frac{d^3 p_{a_i}}{2E_{a_i} (2\pi)^3} e^{-\frac{E_{a_i}}{T}} \right] \\ &\quad \times \prod_{f_j} \left[ \int \frac{d^3 p_{f_j}}{2E_{f_j} (2\pi)^3} \right] \times (2\pi)^4 \delta^4 \left( p_\chi + \sum_{i=1}^n p_{a_i} - \sum_{j=1}^m p_{f_j} \right) |M|^2, \end{aligned} \quad (3)$$

where  $|M|^2$  is the squared amplitude summed over the initial and final spins in the presence of fermions. Note that in this work we always assume the absence of tree-level CP violation, and hence  $\gamma^{\text{eq}}(ij \cdots \rightarrow k\chi \cdots) = \gamma^{\text{eq}}(k\chi \cdots \rightarrow ij \cdots)$ . For  $2 \leftrightarrow 2$  processes, the thermal rate can be succinctly expressed as [81]

$$\gamma^{\text{eq}}(a_1 a_2 \leftrightarrow f_1 f_2) = \frac{T}{64\pi^4} \int_{s_{\text{min}}}^{\infty} ds \sqrt{s} \hat{\sigma}(s) K_1 \left( \frac{\sqrt{s}}{T} \right), \quad (4)$$

where  $s$  is the squared center-of-mass energy and  $s_{\text{min}} = \max[(m_{a_1} + m_{a_2})^2, (m_{f_1} + m_{f_2})^2]$ . The symbol  $\hat{\sigma}$  is the reduced cross-section defined as  $\hat{\sigma} \equiv 2s \lambda(1, m_{a_1}^2/s, m_{a_2}^2/s) \sigma$ , where  $\sigma$  is the cross-section, summed over the initial and final spins, and  $\lambda$  is the phase-space function:  $\lambda[a, b, c] \equiv (a - b - c)^2 - 4bc$ . On the other hand, for the decay of the particle  $a_1$ , the thermal rate becomes [81]

$$\gamma^{\text{eq}}(a_1 \leftrightarrow f_1 f_2) = n_{a_1}^{\text{eq}} \frac{K_1(z)}{K_2(z)} \Gamma_{a_1}, \quad (5)$$

where  $z = m_{a_1}/T$ ,  $\Gamma_{a_1}$  is the decay width of  $a_1$  at rest, and  $K_i$  refers to the modified Bessel function of the  $i$ -th kind.

To account for the observed DM relic density,  $\Omega_{\text{DM}} = 0.26$  [1, 2], the requisite number density in the comoving frame is

$$Y_{\text{DM}}(z \rightarrow \infty) = \frac{4.32 \times 10^{-10}}{(m_{\text{DM}}/\text{GeV})}, \quad (6)$$

where  $m_{\text{DM}}$  is the DM mass.

### III. A SIMPLE MODEL AND THE SEQUENCE OF ASYMMETRY TRANSFER

In this Section, we present a model which can accommodate two-component ADM  $\chi$  and  $\psi$  with very different masses of  $\sim \text{GeV}$  and  $\gtrsim 100 \text{ GeV}$  respectively, followed by detailed discussions on how the asymmetry is transferred among the different particle species.

#### A. Model

There exist two dark sectors that contain vector-like fermion  $\psi$  and  $\chi$  respectively, both of which carry a charge of  $+1$  under a global  $U(1)'$  symmetry but are singlets under the SM gauge groups. The  $U(1)'$  charge ensures the DM stability because all SM particles are neutral under the  $U(1)'$ . These two DM sectors are individually in thermal equilibrium with the SM sector via interactions of  $\bar{\chi}\chi, \bar{\psi}\psi \leftrightarrow \bar{f}f$  that are assumed to be efficient enough to deplete the symmetric components of  $\chi$  and  $\psi$ . Additionally, there are two scalars  $\phi$  (real) and  $\phi'$  (complex). The particle  $\phi$  is a pure singlet, and mediates the long-range interactions among  $\psi$  and  $\bar{\psi}$  particles, resulting in bound state formation (BSF),  $i + j \rightarrow [ij] + \phi$  ( $i$  and  $j$  are referring to  $\psi$  and/or  $\bar{\psi}$ , and  $[ij]$  is the bound state made of the fields  $i$  and  $j$ ) and the inverse process, bound state dissociation (BSD). On the other hand,  $\phi'$  has a  $U(1)'$  charge of  $-2$  and induces interactions that can shift asymmetry between  $\chi$  and  $\psi$ <sup>2</sup>. The particle contents are summarized in Table I. The relevant Lagrangian reads

$$\begin{aligned} \mathcal{L} \supset & -y\phi\bar{\psi}\psi - y'\phi\bar{f}f - \kappa_\chi\phi'\bar{\chi}^c\chi - \kappa_\psi\phi'\bar{\psi}^c\psi + \frac{\bar{\chi}\gamma^\mu\chi\bar{f}\gamma_\mu f}{\Lambda_\chi^2} + \frac{\bar{\psi}\gamma^\mu\psi\bar{f}\gamma_\mu f}{\Lambda_\psi^2} \\ & - m_\chi\bar{\chi}\chi - m_\psi\bar{\psi}\psi - \frac{1}{2}m_\phi^2\phi^2 - m_{\phi'}^2\phi'^*\phi' \end{aligned} \quad (7)$$

where the superscript  $c$  denotes charge conjugate that explicitly indicates that the  $\phi'$ -Yukawa interactions engender the asymmetry transfer,  $\chi\chi$  ( $\bar{\chi}\bar{\chi}$ )  $\leftrightarrow \psi\psi$  ( $\bar{\psi}\bar{\psi}$ ). The two four-fermion effective operators characterize interactions between DM and SM fermions ( $f$ ), mediated by an unspecified heavy gauge boson. These interactions not only keep both  $\chi$  and  $\psi$  in the thermal bath but also eliminate the symmetric components of  $\chi$  and  $\psi$ <sup>3</sup> when  $T \lesssim m_\chi, m_\psi$

<sup>2</sup> Instead of including  $\phi'$ , one can assume feeble  $\psi\psi \rightarrow \bar{f}f$  which breaks the  $U(1)'$  symmetry and makes the bound state decay at a later time, reducing  $Y_\psi$  to achieve  $\Omega_\psi \sim \Omega_\chi$ . In this case, the stability of  $\psi$  is still protected by a residual  $Z_2$  symmetry. Notwithstanding, the freeze-in process of  $\psi\psi \rightarrow \chi\chi$  under consideration can give rise to boosted  $\chi$  which entails rich phenomenological consequences.

<sup>3</sup> The heavy component  $\psi$  has an additional annihilation channel  $\bar{\psi}\psi \rightarrow \phi\phi$ .

which leads to ADM. For  $m_\chi \sim \text{GeV}$  and  $m_\psi \sim \text{TeV}$ , one requires  $\Lambda_\chi \lesssim 350 \text{ GeV}$  and  $\Lambda_\psi \lesssim 6.5 \text{ TeV}$ . to annihilate away the symmetric components. To avoid or mitigate potential experimental constraints on the underlying gauge boson, one can simply assume the gauge boson only couples to the third-generation SM fermions. The identity of the gauge boson and the details of the interactions are not relevant to our discussions as long as the resulting cut-off scales  $\Lambda_\chi$  and  $\Lambda_\psi$  are small enough to keep the interactions in equilibrium.

The Yukawa coupling  $y'$  leads to decays of  $\phi$  into SM fermions<sup>4</sup> if kinematically allowed as well as keeping  $\phi$  in thermal equilibrium until  $T$  drops well below  $m_\phi$ . As mentioned

|          | $\chi$                    | $\psi$                                 | $\phi$                | $\phi'$        |
|----------|---------------------------|--|-----------------------|----------------|
| Mass     | $\mathcal{O}(\text{GeV})$ | $\mathcal{O}(\gtrsim 100 \text{ GeV})$ | $\lesssim \text{GeV}$ | $> \text{TeV}$ |
| $U(1)_D$ | +1                        | +1                                     | 0                     | -2             |

TABLE I: The particle contents in the dark sectors where all particles are singlets under the SM gauge groups. See the text for details.

above, the bound states form in the  $\psi$  sector due to the Yukawa interaction of  $\phi$ . Since the interaction is always attractive among particles and antiparticles, there exist three types of the bound states:  $R_{\psi\psi}$  ( $\sim [\psi\psi]$ ),  $R_{\bar{\psi}\bar{\psi}}$  ( $\sim [\bar{\psi}\bar{\psi}]$ ) and  $R_{\bar{\psi}\psi}$  ( $\sim [\bar{\psi}\psi]$ ). In the limit of  $m_\phi \ll y^2 m_\psi / (8\pi)$  (inverse of the Bohr radius), the Yukawa potential can be well approximated by a Coulomb potential. This approximation greatly simplifies the calculations on the cross-sections of BSF and BSD, that are summarized in Appendix B. In this work, we consider only the ground state with a binding energy:

$$E_B = -\frac{y^4}{64\pi^2} m_\psi + \frac{y^2}{4\pi} m_\phi. \quad (8)$$

The bound state mass is  $m_R = 2m_\psi + E_B$ , with  $m_{R_{\psi\psi}} = m_{R_{\bar{\psi}\bar{\psi}}} = m_{R_{\bar{\psi}\psi}} \equiv m_R$ .

The bound states themselves will not be stable as  $R_{\bar{\psi}\psi}$  will quickly decay either into a pair of  $\phi$  induced by the  $\phi$ -Yukawa interaction or into SM fermions via the annihilations of  $\psi$  and  $\bar{\psi}$ , while  $R_{\psi\psi}$  ( $R_{\bar{\psi}\bar{\psi}}$ ) will eventually decay into a pair of  $\chi$  ( $\bar{\chi}$ ) through the feeble interactions  $\chi\chi \leftrightarrow \psi\psi$  ( $\bar{\chi}\bar{\chi} \leftrightarrow \bar{\psi}\bar{\psi}$ ). In light of the asymmetry of  $\psi$ , only  $R_{\psi\psi}$  ( $R_{\bar{\psi}\bar{\psi}}$ ) exists

<sup>4</sup> The coupling can arise, e.g., via the mixing between the SM Higgs boson and  $\phi$ , leading to  $y' \approx y_f^{\text{SM}} \sin \theta$ , where  $\theta$  is the mixing angle and  $y_f^{\text{SM}}$  is the SM Yukawa coupling. To ensure  $\phi$  is in the thermal bath for  $T \lesssim m_\phi \sim \text{GeV}$  (scale of interest in this work), we have  $y' \gtrsim 10^{-9}$ , indicating  $\sin \theta \gtrsim 10^{-7}$ , depending on the final state fermions. Such a small mixing angle is well below the current experimental sensitivity.

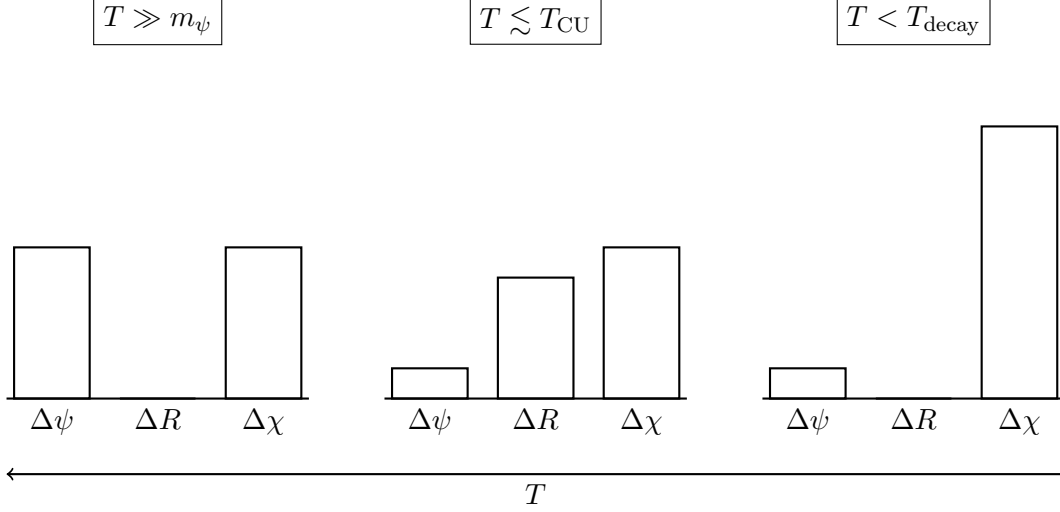


**Figure 1:** Illustration of the asymmetry transfer between the heavy ( $\psi$ ) and light ( $\chi$ ) components with the help of the bound states  $R$ . At a high temperature, an asymmetry is generated and shared by both the dark and SM sectors. Below the temperature  $T_{\text{CU}}$  (catch-up temperature at which  $Y_R = Y_\psi/2$ ), more than half of the  $\psi$  asymmetry has been stored in the bound states. The bound states later decay into  $\chi$ , thereby transferring the majority of the asymmetry from  $\psi$  into  $\chi$ , leading to  $Y_\chi \gg Y_\psi$  but with  $\Omega_\chi \approx \Omega_\psi$  as  $m_\psi \gg m_\chi$ .

for  $T \ll m_\psi$  in case  $Y_\psi > Y_{\bar{\psi}}$  ( $Y_\psi < Y_{\bar{\psi}}$ ) initially. All relevant cross-sections and decay rates are given in Appendix A.

In the following numerical analysis, we solve the Boltzmann equations for the species  $\phi$ ,  $\psi$ ,  $\bar{\psi}$ ,  $R_{\psi\psi}$ ,  $R_{\bar{\psi}\bar{\psi}}$  and  $R_{\psi\bar{\psi}}$  by including the interactions of BSF, BSD,  $\bar{\psi}\psi \leftrightarrow \bar{f}f$ ,  $\bar{\psi}\psi \leftrightarrow \phi\phi$ ,  $R_{\bar{\psi}\bar{\psi}} \leftrightarrow \phi\phi$ ,  $R_{\psi\psi} \leftrightarrow \chi\chi$  ( $R_{\bar{\psi}\bar{\psi}} \leftrightarrow \bar{\chi}\bar{\chi}$ ) and  $\phi \leftrightarrow \bar{f}f$ .

## B. Asymmetry transfer

We here elaborate in detail on how the initial asymmetry is transferred between the  $\chi$  and  $\psi$  sector as the universe cools down. The sequence of the asymmetry transfer via BSF and BSD is pictorially illustrated in Fig. 1. The time evolution of the densities of the relevant species are shown in Fig. 2, in which for demonstration we choose  $(m_\psi, m_{\phi'}, \Lambda_\psi) = (1, 10, 10)$  TeV with massless  $\phi$  and  $f$ , and  $(y, \kappa_\chi, \kappa_\psi) = (1, 10^{-4}, 10^{-4})$ , implying a binding energy of  $|E_B| = 1.58$  GeV. The solid green (red, blue) line corresponds to  $Y_\phi$  ( $Y_\psi$ ,  $Y_{R_{\psi\psi}}$ ) while the



dashed red (blue) line represents  $Y_{\bar{\psi}}$  ( $Y_{R_{\bar{\psi}\bar{\psi}}}$  and  $Y_{R_{\bar{\psi}\psi}}$ <sup>5</sup>). The vertical dashed grey lines mark the absolute value of the binding energy and the catch-up temperature, defined below. For  $T \lesssim 10^{-2}$  GeV, the light (dark) blue line refer to the case of stable (decaying)  $R_{\psi\psi}$ .

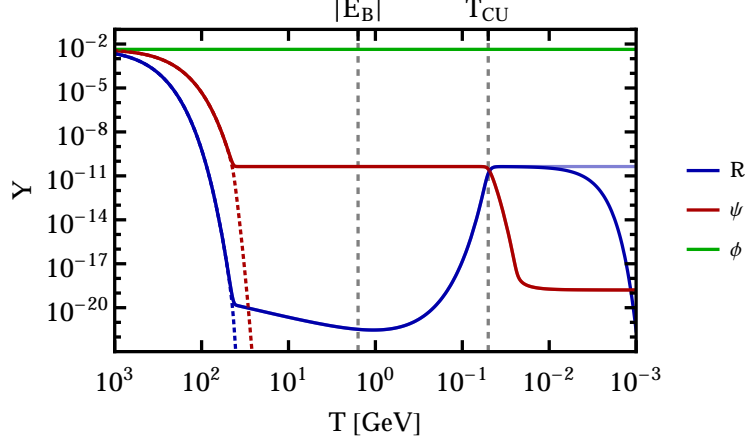


**Figure 2:** The time evolution of the densities for particles in the dark sectors, where  $(m_\psi, m_{\phi'}, \Lambda_\psi) = (1, 10, 10)$  TeV with massless  $\phi$  and  $(y, \kappa_\chi, \kappa_\psi) = (1, 10^{-4}, 10^{-4})$  are assumed. The solid green (red, blue) line represents  $Y_\phi$  ( $Y_\psi$ ,  $Y_{R_{\psi\psi}}$ ). The dashed red (blue) line refers to  $Y_{\bar{\psi}}$  ( $Y_{R_{\bar{\psi}\bar{\psi}}}$  and  $Y_{R_{\bar{\psi}\psi}}$ ), demonstrating that the symmetric components are annihilated away. The horizontal light blue line at small  $T$  stands for the case of stable  $R_{\psi\psi}$  without decaying into  $\chi$ , while the final density of  $\psi$  (red line) is unaffected by the decay as BSF already stops before the decay.

- At  $T \gg m_\psi$ ,  $\chi$  and  $\psi$  are individually in thermal equilibrium with the SM. An unspecified mechanism is presumed for generating asymmetries in all  $\chi$ ,  $\psi$  and the SM baryons (e.g., out-of-equilibrium decays of heavy gauge or Higgs bosons [82–85]). For simplicity, we assume that the total initial asymmetry of the three sectors adds up to zero:

$$\Delta Y_B + \Delta Y_\psi^i + \Delta Y_\chi^i = 0, \quad (9)$$

in which the superscript  $i$  refers to the initial values and  $\Delta Y_f \equiv Y_f - Y_{\bar{f}}$ . Furthermore, it is assumed that the generated baryon asymmetry accounts for the observed value, i.e.  $\Delta Y_B = (8.6 \pm 0.7) \times 10^{-11}$  [2] and remains constant once being created<sup>6</sup>. In this

<sup>5</sup> The lines corresponding to  $Y_{R_{\bar{\psi}\bar{\psi}}}$  and  $Y_{R_{\bar{\psi}\psi}}$  are on top of each other.

<sup>6</sup> In fact, our conclusions do not rely on these assumptions.

work, we set  $\Delta Y_\psi^i \sim \Delta Y_\chi^i > 0$ , namely there are more  $\psi$  ( $\chi$ ) than  $\bar{\psi}$  ( $\bar{\chi}$ ).

- Depending on the binding energy and the mass of  $\phi$ , BSF and BSD are virtually efficient for a large part of the time period of interest. From Eq. (2), it implies

$$\frac{n_\psi^2}{(n_\psi^{\text{eq}})^2} \approx \frac{n_{R_{\psi\psi}}}{n_{R_{\psi\psi}}^{\text{eq}}} \frac{n_\phi}{n_\phi^{\text{eq}}}. \quad (10)$$

That in turn indicates  $R$  also follows its equilibrium density when  $T \gtrsim m_\psi$  because both  $\psi$  and  $\phi$  are in thermal equilibrium.

- For  $|E_B| \lesssim T \lesssim m_\psi$ , the annihilations of  $\bar{\psi}$  and  $\psi$  into  $\phi$  and SM fermions are kinematically more favorable than the reverse reactions and thus the number density of  $\psi$  experiences a Boltzmann suppression. At a certain point, the equilibrium number density of  $\psi$  becomes smaller than the asymmetry stored in  $\psi$ . It indicates that the symmetric component has been mostly obliterated and what remains is the asymmetric component –  $\psi$  particles. The depletion of the symmetric component of the bound states also takes place roughly at the same time as  $\psi$  since the number densities are connected by Eq. (10). In our example, it happens around  $T = 41 \text{ GeV}$  but with  $Y_{R_{\psi\psi}} \ll Y_\psi$  because the former suffers a double Boltzmann suppression due to  $\exp(-m_R/T) \approx \exp(-2m_\psi/T) \ll \exp(-m_\psi/T)$ . Alternatively, the relative suppression can be understood by inspecting Eq. (10):  $n_R \sim (m_\psi T)^{-3/2} (n_\psi)^2 \ll n_\psi$ , given  $n_\phi = n_\phi^{\text{eq}}$ .
- At  $T \lesssim |E_B| + m_\phi$ , the density  $Y_{R_{\psi\psi}}$  increases sharply, catching up with  $Y_\psi$ , as clearly shown in Fig. 2. One can apprehend the catch-up behavior via the interplay between BSF and the conservation of the total asymmetry as follows. While the process of  $\psi\psi \leftrightarrow R_{\psi\psi} \phi$  can change the number densities of  $R_{\psi\psi}$  and  $\psi$  individually, the total asymmetry stays constant before the decay of  $R_{\psi\psi}$ :

$$\Delta Y_\psi^i = Y_\psi + 2Y_R. \quad (11)$$

Furthermore, as long as the interaction  $\phi \bar{f} f$  in Eq. (7) is faster than the expansion rate of the universe,  $\phi$  is in equilibrium, implying  $n_\phi = n_\phi^{\text{eq}}$ . As a result, combining Eq. (10) and (11), one obtains an analytic expression for the number density of  $R_{\psi\psi}$ ,

provided that BSF and BSD are effective:

$$Y_R = \frac{\Delta Y_\psi^i}{2} + \mathcal{R} \left( 1 - \sqrt{1 + \frac{\Delta Y_\psi^i}{\mathcal{R}}} \right), \quad (12)$$

with

$$\mathcal{R} = \frac{(n_\psi^{\text{eq}})^2}{8n_R^{\text{eq}}s_{\text{en}}}. \quad (13)$$

The equilibrium number densities of the non-relativistic  $\psi$  and  $R_{\psi\psi}$  scale as  $n^{\text{eq}} \sim (mT)^{\frac{3}{2}} \exp(-\frac{m}{T})$ . That implies  $\mathcal{R} \sim (m_\psi/T)^{-\frac{3}{2}} \exp(-\frac{|E_B|}{T}) \rightarrow 0$  in the limit of  $T \rightarrow 0$ , and consequently  $Y_R \stackrel{T \rightarrow 0}{=} \frac{\Delta Y_\psi^i}{2}$ . In other words, BSF is favored over BSD and most of the asymmetry would be transferred to the bound states. The underlying reason is that more and more  $\phi$  particles no longer have sufficient energy to overcome the binding energy (a requirement to break the bound state), when the temperature falls below  $|E_B|$ . With a larger Yukawa coupling (larger  $|E_B|$ ), more  $\psi$  particles will be converted into  $R_{\psi\psi}$ , leading to more asymmetry being stored in  $\chi$  after  $R_{\psi\psi}$  decays. That is why the existence of the bound states naturally allows for two-component ADM of very different mass scales but with comparable energy densities. In fact, the situation here is very similar to the one during recombination at which electrons and protons first became bound to form neutral hydrogen atoms. In case  $\phi$  is massive, its number density also has an exponential suppression at  $T < m_\phi$  such that in the end there are not enough  $\phi$  particles to fragment the bound states, rendering BSD ineffective.

- We define the catch-up temperature  $T_{\text{CU}}$  as the temperature when the asymmetry is equally shared by  $R_{\psi\psi}$  and free  $\psi$ , i.e.,  $Y_\psi/2 = Y_{R_{\psi\psi}}$  at  $T = T_{\text{CU}}$ . By setting  $Y_R = \Delta Y_\psi^i/4$  in Eq. (12), the value of  $T_{\text{CU}}$  can be numerically calculated. In our exemplary case shown in Fig. 2, we have  $T_{\text{CU}} = 0.05$  GeV. With  $m_\phi = 0$ , an empirical expression of  $T_{\text{CU}}$  for  $0.1 \lesssim y \lesssim 5$  can be found as

$$T_{\text{CU}} \approx 0.03 |E_B| y^{1/5}, \quad (14)$$

with an accuracy above 90 %.

- As more and more  $\psi$  particles are being converted, it becomes harder and harder for them to find each other to form the bound state. Eventually below a certain temperature, denoted by  $T_{\text{D}}$ , the precise value of which is determined by the parameters  $m_\phi$

and  $y$ , BSF ceases to work, similar to the freeze-out of thermal DM. In our example,  $T_D$  is around 12 MeV below which  $Y_\psi$  stops decreasing and levels off as shown in Fig. 2. The asymmetry stored in the bound states after the asymmetry transfer is given by  $Y_{R_{\psi\psi}}(T_D)$ , while the final asymmetry stored in  $\psi$ , represented by  $\Delta Y_\psi^f$ , is simply  $Y_\psi(T_D)$ . After the decay of  $R_{\psi\psi}$ , the final  $\chi$  asymmetry is:

$$\Delta Y_\chi^f = -\Delta Y_B - \Delta Y_\psi^f, \quad (15)$$

where we have used Eq. (9) and

$$\Delta Y_\chi^i + \Delta Y_\psi^i = \Delta Y_\chi^f + \Delta Y_\psi^f. \quad (16)$$

As a result, the ratio of the total energy density of DM to that of the SM baryons reads

$$\frac{\Omega_{\text{DM}}}{\Omega_B} = \left| \frac{\Delta Y_\psi^f}{\Delta Y_B} \right| \frac{m_\psi - m_\chi}{m_B} + \frac{m_\chi}{m_B}, \quad (17)$$

and in order to reproduce the observed relic density one has

$$\left| \frac{\Delta Y_\psi^f}{\Delta Y_B} \right| = \frac{m_B}{m_\psi - m_\chi} \left( \frac{\Omega_{\text{DM}}}{\Omega_B} - \frac{m_\chi}{m_B} \right) \stackrel{m_\psi \gg m_\chi}{=} \frac{m_\chi}{m_\psi} \left[ \frac{m_B}{m_\chi} \frac{\Omega_{\text{DM}}}{\Omega_B} - 1 \right]. \quad (18)$$

If we further require that the energy densities of  $\psi$  and  $\chi$  are comparable ( $m_\psi \Delta Y_{\psi,f} \sim m_\chi \Delta Y_{\chi,f}$ ), the mass of  $\chi$  can be inferred

$$m_\chi \sim \frac{m_\psi m_B}{2m_\psi - m_B} \frac{\Omega_{\text{DM}}}{\Omega_B} \stackrel{m_\psi \gg m_B}{=} m_B \frac{\Omega_{\text{DM}}}{2\Omega_B} = 2.66 \text{ GeV}, \quad (19)$$

that indicates

$$\left| \frac{\Delta Y_\psi^f}{\Delta Y_B} \right| \sim \frac{m_\chi}{m_\psi}, \quad (20)$$

given  $\Omega_{\text{DM}} = 5.4 \Omega_B$  and  $m_B \approx 1 \text{ GeV}$ . Therefore, the final density of  $\psi$  (solid red line) in Fig. 2 is too small to have any impact on the relic density.

To sum up, when the temperature falls below  $m_\psi$ , the symmetric components of  $\psi$  and  $R$  will be destroyed by the processes of  $\bar{\psi}\psi \rightarrow \phi\phi$ ,  $\bar{f}f$  and  $R_{\bar{\psi}\psi} \rightarrow \phi\phi$ , and only the asymmetric component, comprising  $\psi$  and  $R_{\psi\psi}$ , is left with  $Y_\psi \gg Y_{R_{\psi\psi}}$  in light of the Boltzmann suppression. At  $T \lesssim |E_B|$ ,  $Y_{R_{\psi\psi}}$  begins to catch up with  $Y_\psi$  due to the lack of energetic

$\phi$  to dissociate the bound state, i.e., BSF being kinematically preferred over BSD. With the continuous decrease in  $Y_\psi$ , BSF will ultimately become ineffective as the BSF rate is proportional to  $Y_\psi^2$ . Afterwards, the density  $Y_\psi$  stays constant while the bound state decays into a pair of  $\chi$ . The Yukawa coupling  $y$  determines when BSF stops and therefore the final value of  $Y_\psi$ . In the following, we will discuss the sufficient conditions for realizing two-component ADM with comparable energy densities but very different mass scales between the two DM components. Throughout our analyses, we always assume  $m_\chi = 2.66$  GeV unless otherwise stated.

#### IV. NUMERICAL RESULTS

In this Section we present numerical solutions of the coupled Boltzmann equations involving (anti-)particles of  $\psi$  and  $R$  as well as  $\phi$ . We investigate how the Yukawa coupling  $y$ , the mediator mass  $m_\phi$  and the decay width  $\Gamma_{R_{\psi\psi}}$  individually influence the final amounts of asymmetry stored in  $\psi$  and  $R_{\psi\psi}$  ( $\chi$ ). Finally, we present four benchmark scenarios with different  $m_\psi$  but fixed  $m_\chi$ , where the correct relic density is reproduced with  $\Omega_\chi \approx \Omega_\psi$ .

##### A. Effect of $y$ values

In Fig. 3 we show the impact of different Yukawa couplings  $y = (0.2, 0.3, 0.4)$  on the final number densities, assuming massless  $\phi$ , TeV  $\psi$  and a stable bound state with an initial condition of  $\Delta Y_\psi^i = \Delta Y_B$  at high  $T$ . Clearly, the final abundance of  $\psi$  decreases as  $y$  increases. Since the BSF cross-section scales as  $y^{12}$ , a larger Yukawa coupling corresponds to a much larger BSF rate and thus more  $\psi$  form bound states, implying a smaller final density of  $\psi$ . On the other hand, from Eq. (14) the catch-up temperature is proportional to  $|E_B|y^{1/5} \sim y^{21/5}$  and hence larger  $y$  indicates an earlier catch-up as shown in Fig. 3. In the case of  $y = 0.2$ , the BSF processes even cease to work prior to the catch-up. As a consequence, to reproduce the correct relic density, most of the  $\psi$  asymmetry has to be transferred into the bound state, setting a lower bound on the value of  $y$ .

Given  $m_\chi = 2.66$  GeV and  $m_\psi = 1$  TeV, the value of  $y \sim 0.33$  is required to reproduce a correct value of  $\Delta Y_\psi^f$  that fulfills Eq. (20) and in turn attains  $\Omega_\psi \sim \Omega_\chi$ . The corresponding plummet of  $Y_\psi$  (surge on  $Y_{R_{\psi\psi}}$ ) takes place between those of  $y = 0.3$  and  $y = 0.4$ , i.e, around

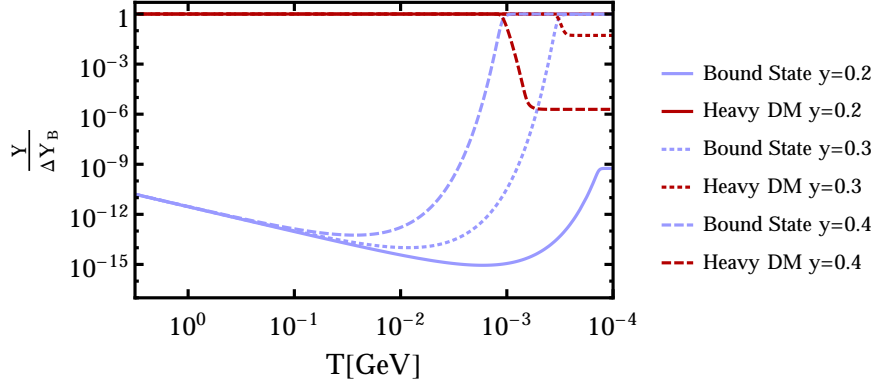


**Figure 3:** The results of the Boltzmann equations for different Yukawa couplings  $y = (0.2, 0.3, 0.4)$ , given  $m_\chi = 2.66$  GeV,  $m_\psi = 1$  TeV and  $\Gamma_{R_{\psi\psi}} = 0$  with massless  $\phi$ . The red (blue) lines represent the number density of  $\psi$  ( $R_{\psi\psi}$ ) normalized to the baryon density. The different line styles correspond to the different values of  $y$ . Comparable densities  $\Omega_\chi \approx \Omega_\psi$  can be accommodated by taking  $y \approx 0.33$ . The initial condition of  $\Delta Y_\psi^i = \Delta Y_B$  at large  $T$  is presumed.

$T \lesssim 1$  MeV. The bound states will eventually decay, creating a population of highly energetic  $\chi$  particles below the scale of Big Bang nucleosynthesis (BBN). Moreover, if the presumed asymmetry generation mechanism instead creates more  $\bar{\chi}$  than  $\chi$ , then annihilations of induced  $\chi$  with pre-existing  $\bar{\chi}$  into the SM fermions will also inject sizable entropy into the thermal bath and thus the model will be constrained by BBN measurements. See, for instance, Refs. [86–88].

Since most of the bound states are produced around  $T = T_{\text{CU}}$ , in order not to perturb BBN we have to raise  $T_{\text{CU}}$  above the scale of MeV such that the subsequent decay of the bound state can happen before the onset of BBN. Naively thinking, one may enlarge  $y$ , which in return leads to an earlier catch-up and also puts an end to BSF above the BBN scale. The increase on  $y$ , nonetheless, will also decrease significantly the final density  $Y_\psi$  – there is a difference of more than four orders of magnitude in  $Y_\psi^f$  between the cases of  $y = 0.3$  and  $y = 0.4$ , resulting in  $\left| \Delta Y_\psi^f / \Delta Y_B \right| \ll m_\chi / m_\psi$  and hence  $\Omega_\psi \ll \Omega_\chi$ . One possible solution is to make  $\phi$  massive in combination with a large value of  $y$  as discussed below.

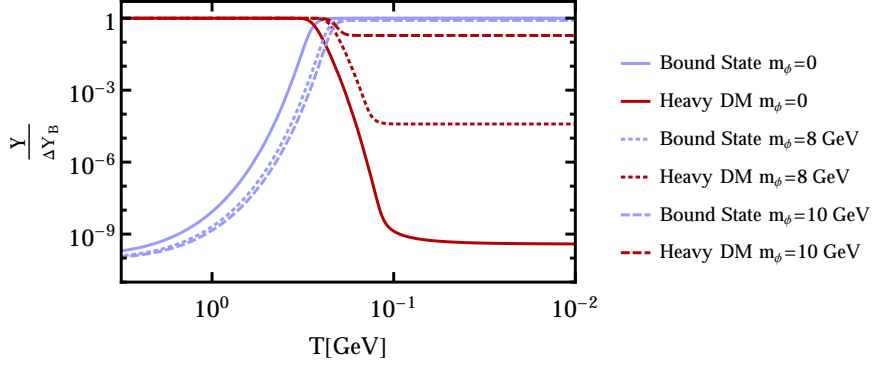


**Figure 4:** The solutions of the Boltzmann equations for  $m_\psi = 1$  TeV,  $y = 1.5$  and the different values of  $m_\phi = (0, 8, 10)$  GeV. The binding energy, that partially depends on  $m_\phi$  as shown in Eq. (8), is around 8 GeV. The red (blue) lines represent the number density of  $\psi$  ( $R_{\psi\psi}$ ) normalized to the baryon asymmetry. The different styles of the lines correspond to the different mediator masses. The density  $Y_\psi^f$  increases with larger  $m_\psi$ , and the mass dependence is very striking.

### B. Effect of a non-zero mediator mass

The final densities of  $\psi$  and  $R_{\psi\psi}$  depend on the value of decoupling temperature  $T_D$  below which BSF stops. In case of a massless  $\phi$ , the BSF process  $\psi\psi \rightarrow R_{\psi\psi}\phi$  is always kinematically allowed ( $2m_\psi > m_R$ ) but it becomes ineffective when  $Y_\psi$  is diminutive, as explained above. To obtain a large value of  $Y_\psi^f$ , it is necessary to halt BSF earlier. With  $m_\phi > |E_B|$ , in addition to the Boltzmann suppression from the density  $n_\psi$ , BSF will also have a kinematical suppression by virtue of  $2m_\psi < m_R + m_\phi$  when  $T < m_\phi$ , leading to a higher  $T_D$  and hence a larger  $Y_\psi^f$ . In Fig. 4, it is clear that a larger mass of  $\phi$  gives rise to a larger final density of  $\psi$  where we fix  $y = 1.5$  and  $m_\psi = 1$  TeV with the same initial condition  $\Delta Y_\psi^i = \Delta Y_B$  as above. The dependence of the final density  $Y_\psi^f$  on the mass  $m_\phi$  is quite remarkable – increasing  $m_\phi$  from 8 to 10 GeV is accompanied by a factor of nearly  $10^4$  on the final density.

On the other hand, the temperature  $T_{CU}$  becomes lower in the presence of massive  $\phi$  as shown in Fig. 4. That can be understood by noticing that  $Y_{R_{\psi\psi}}$  begins to rise when  $\phi$  no longer has enough energy to break apart the bound states. Due to the fact that the mass of  $\phi$  itself as energy can also be used to destroy the bound states, involving a massive  $\phi$  will postpone the catch-up and thus lower  $T_{CU}$ . As a result, one would need a large value

of  $y$  together with a nonzero mass of  $\phi$  ( $\gtrsim |E_B|$ ) to increase both  $T_{\text{CU}}$  and  $T_{\text{D}}$ , ensuring the majority of the bound states decay before BBN while attaining a sizable final density of  $\psi$ .

### C. Effect of a non-zero Decay Width

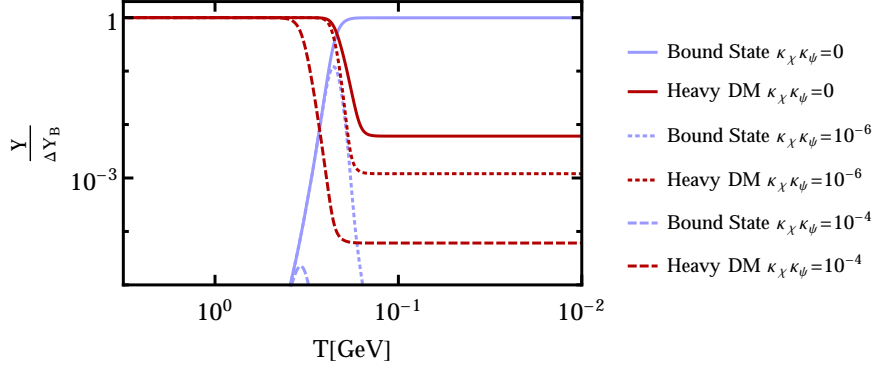


**Figure 5:** The results of the Boltzmann equations, given  $m_\psi = 1 \text{ TeV}$ ,  $m_\phi = 9 \text{ GeV}$ ,  $y = 1.5$  and different values of  $\kappa_\chi \kappa_\psi = (0, 10^{-6}, 10^{-4})$ , that correspond to different decay widths  $\Gamma_{R_{\psi\psi}}$  as  $\Gamma_{R_{\psi\psi}} \sim (\kappa_\psi \kappa_\chi)^2$ . The red (blue) lines represent the number density of  $\psi$  ( $R_{\psi\psi}$ ) normalized to the baryon density.

Lastly, we study the influence of the bound state decay on the final densities of  $\psi$  and  $\chi$ . The effect is illustrated in Fig. 5 with again the same initial condition  $\Delta Y_\psi^i = \Delta Y_B$ . The decay eliminates the bound state population and stops BSD at an earlier time (leads to higher  $T_{\text{CU}}$ ) when compared to situations of stable  $R_{\psi\psi}$ , since there are fewer bound states left over for dissociation. That is to say, only BSF is active and causes more  $\psi$  being converted into the bound states that subsequently decay into  $\chi$ . Note that if the bound state decays only after BSF ceases to function, then the final  $\psi$  density will not be affected by the decay as displayed in Fig. 2.

The decay width of  $R_{\psi\psi}$  is partially controlled by the product of the couplings  $\kappa_\chi$  and  $\kappa_\psi$ . In Fig. 5, the decay takes place during the catch-up period, and a larger decay width corresponds to fewer  $\psi$  but more  $\chi$  particles – increasing the product  $\kappa_\chi \kappa_\psi$  from  $10^{-6}$  to  $10^{-4}$  makes  $Y_\psi^f$  more than ten times smaller. Again, we focus on freeze-in scenarios where  $\psi\psi$  ( $R_{\psi\psi}$ )  $\leftrightarrow \chi\chi$  was not in thermal equilibrium at high  $T$  but only *freezes in* during or after the catch-up period. That imposes constraints on the parameter space as discussed in



## Appendix C.

### D. Benchmark Scenarios

To conclude, we present four benchmark sets of the parameters, listed in Table II, which are capable of reproducing the observed  $\Omega_{\text{DM}}$  with  $\Omega_\chi \approx \Omega_\psi$ . The corresponding time

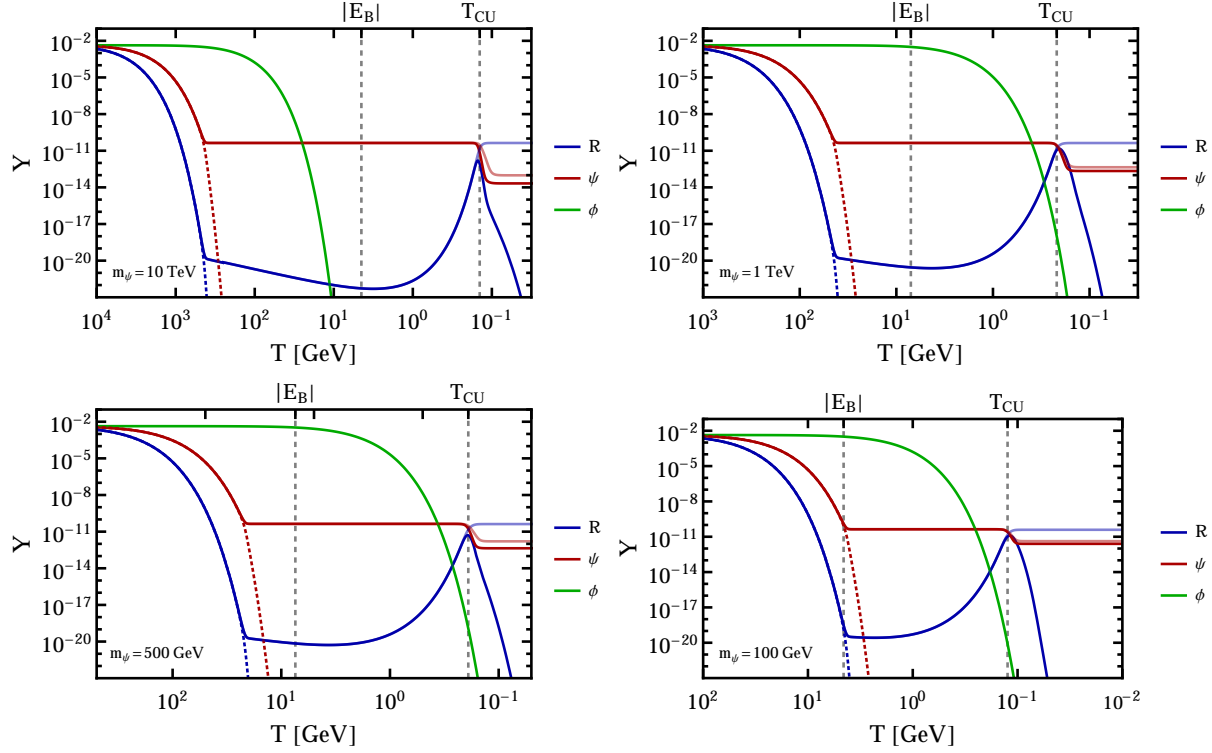
| $m_\chi[\text{GeV}]$ | $m_\psi[\text{GeV}]$ | $m_\phi[\text{GeV}]$ | $m_{\phi'}[\text{GeV}]$ | $y$  | $\kappa_\psi$       | $\kappa_\chi$       |
|----------------------|----------------------|----------------------|-------------------------|------|---------------------|---------------------|
| 2.66                 | 10000                | 5.7                  | 10000                   | 0.75 | $3 \cdot 10^{-4}$   | $3 \cdot 10^{-4}$   |
| 2.66                 | 1000                 | 9                    | 1000                    | 1.5  | $1.2 \cdot 10^{-4}$ | $1.2 \cdot 10^{-4}$ |
| 2.66                 | 500                  | 8.25                 | 500                     | 1.75 | $1.5 \cdot 10^{-4}$ | $1.5 \cdot 10^{-4}$ |
| 2.66                 | 100                  | 5.75                 | 100                     | 2.5  | $7 \cdot 10^{-5}$   | $7 \cdot 10^{-5}$   |

TABLE II: Sets of parameters reproducing the observed relic density with the comparable energy densities between  $\psi$  and  $\chi$ , assuming the initial condition  $\Delta Y_\chi^i = \Delta Y_\psi^i = -\Delta Y_B/2$ .

evolution of the particle densities are shown in Fig. 6, similar to Fig. 2 but with working values of the parameters. The mass of  $\chi$  is fixed at 2.66 GeV, while  $m_\psi$  ranges from 100 GeV to 10 TeV. It is assumed that the initial asymmetry created at  $T \gg m_\psi$  is distributed as  $\Delta Y_\chi^i = \Delta Y_\psi^i = -\Delta Y_B/2$ . The rest of parameters are chosen to fulfill  $\Omega_\chi \approx \Omega_\psi$ .

In order to have  $R_{\psi\psi}$  decay before BBN, it is necessary for  $T_{\text{CU}}$  to be above the BBN scale, i.e.  $T_{\text{CU}} \gtrsim \text{MeV}$ . As the catch-up temperature  $T_{\text{CU}}$  scales as  $|E_B| y^{1/5} \sim m_\psi y^{21/5}$ , for the cases with smaller  $m_\psi$  a larger value of  $y$  is requisite, as demonstrated in Table. II. However, due to the fact that the density  $Y_\psi^f$  is extremely sensitive to  $y$ , as illustrated in Fig. 3, a considerable value of  $y$  will often make the final density of  $\psi$  vanishingly small. Therefore, as discussed in Section IV B, a massive  $\phi$  ( $m_\phi \gtrsim |E_B|$ ) is involved to impede BSF, preventing an utter depletion of  $\psi$ . In fact, we have found for  $m_\psi \lesssim \mathcal{O}(\text{TeV})$ , massive  $\phi$  is requisite to obtain  $\Omega_\chi \sim \Omega_\psi$ .

Lastly, the product  $\kappa_\chi \kappa_\psi$ , that determines the decay width of  $R_{\psi\psi}$ , has to be sizable so that the decay will not interfere with BBN, but it cannot be too large in order to retain the freeze-in decay. In addition, the bound state decay leads to more  $\psi$  being converted into  $\chi$ , as seen by comparing the light (without decay) and dark (with decay) red lines in Fig. 6.



**Figure 6:** The results of the Boltzmann equations with  $m_\psi = 10$  TeV (upper left panel),  $m_\psi = 1$  TeV (upper right),  $m_\psi = 500$  GeV (bottom left) and  $m_\psi = 100$  GeV (bottom right). These plots are similar to Fig. 2 but with  $\Omega_\chi \approx \Omega_\psi$ . We choose  $\Delta Y_{\psi_i} = \Delta Y_{\chi_i} = -\Delta Y_B/2$  as the initial condition at large  $T$ . The symmetric components of  $\psi$  and  $R$  are rapidly depleted via the annihilations into  $\phi$  and the SM fermions. The relative distribution of the final asymmetric components of  $\psi$  and  $R$  is determined by when BSF and BSD decouple. Finally, the bound state decay shifts asymmetry into  $\chi$ .

## V. CONCLUSIONS

As multi-component DM and asymmetric DM (ADM) are interesting subjects on their own, we here explore the possibility of combining these two ideas to have two-component ADM with very different masses: the light component  $\chi$  at the scale of GeV and the heavy component  $\psi$  above the electroweak scale. On the other hand, it is a common feature of existing ADM models that the baryon density (asymmetry) is closely correlated with that of DM, and quite often the amounts of asymmetry stored in the DM and SM sectors are of the same order, implying the DM mass is of order  $\mathcal{O}(\text{GeV})$  given  $\Omega_{\text{DM}} = 5.4 \Omega_B$ . In the framework of two-component ADM, if an asymmetry created at an early time is equally

shared among  $\chi$ ,  $\psi$  and the SM baryons, the energy density of the heavy  $\psi$  alone will certainly exceed the observed relic abundance.

A simple solution proposed in this work is to involve a Yukawa-type long-range interaction, mediated by a scalar  $\phi$ , in the sector of  $\psi$ . We always assume that the underlying mechanism of the asymmetry generation creates more  $\chi$  and  $\psi$  than  $\bar{\chi}$  and  $\bar{\psi}$ , but our conclusions do not depend on this assumption. Three types of bound states will form:  $R_{\psi\psi}$ ,  $R_{\bar{\psi}\bar{\psi}}$ , and  $R_{\bar{\psi}\psi}$ , where the subscript denotes the bound state constituents. The densities of the bound states and free  $\psi$  are determined by the interplay between bound state formation and dissociation (BSF and BSD)  $i + j \leftrightarrow R_{ij} + \phi$  for  $(i, j) = \psi$  and/or  $\bar{\psi}$ . The presence of the bound states can facilitate removing the symmetric component of  $\psi$ , preserve the asymmetric component and finally convert most of the asymmetry into  $\chi$  via the late decay of  $R_{\psi\psi} \rightarrow \chi\chi$ .

To be more concrete, when the temperature becomes smaller than the mass of  $\psi$ , most of the symmetric component will be depleted and only the asymmetric component, consisting of  $\psi$  and  $R_{\psi\psi}$ , remains with very different number densities  $n_\psi \gg n_{R_{\psi\psi}}$  due to the Boltzmann suppression. As the temperature further drops below the binding energy of the bound state,  $\phi$  no longer has sufficient energy to break the bound states. Thus BSF is kinematically favored over BSD, making the density  $n_{R_{\psi\psi}}$  catch up with  $n_\psi$ . As BSF proceeds, more and more  $\psi$  particles have been converted and the process eventually stops because the interaction rate is proportional to  $n_\psi^2$ . In the mean time, the bound state starts to decay into  $\chi$ . As a result, the final density of  $\psi$  can be much smaller than that of  $\chi$  while their energy densities are comparable, i.e., two-component ADM.

However, the late decay of the bound states creates a population of energetic  $\chi$  and injects entropy into the thermal bath at  $T \lesssim \text{MeV}$ , that will disturb BBN. To circumvent the issue, one can increase the Yukawa coupling, responsible for the long-range interaction, and involve a massive mediator  $\phi$ . A larger coupling implies a larger binding energy that makes the bound state catch-up occur earlier. In this case, the following decay of the bound state can take place before BBN. On the other hand, a larger value of  $y$  also implies a longer BSF epoch and a further depletion on the final density of  $\psi$  (analogous to thermal DM: a larger coupling between DM and SM particles implies a smaller relic density), resulting in  $\Omega_\psi \ll \Omega_\chi$  and thwarting the attempt on two-component ADM. The undesirable effect of large  $y$ , nonetheless, can be undone by making  $\phi$  massive. With the mass of  $\phi$  being larger

than the binding energy, it costs  $\psi$  energy to form the bound states due to  $2m_\psi < m_R + m_\phi$  and therefore BSF will stop earlier, leaving a sizable population of  $\psi$ .

To conclude, we provide an interesting mechanism to achieve two-component ADM with very different masses but comparable energy densities by involving the long-range interaction and late decay in the heavy component sector. In the follow-up, we will investigate phenomenological implications of this scenario, including boosted DM and DM searches in direct detection.

### Acknowledgments

We would like to thank Joachim Brod for precious contributions at the early stage of this work, and Martin Gorbahn for very helpful but destructive comments on our previous ill-fated model. We are grateful for helpful comments on the draft from Yue-Lin Sming Tsai and Julia Harz. WCH was supported by the Independent Research Fund Denmark, grant number DFF 6108-00623. The CP3-Origins centre is partially funded by the Danish National Research Foundation, grant number DNRFF90. MB would like to thank Heinrich Päs for providing the possibility to work on this project and his constant support throughout the work.

### Appendix A: Relevant reduced cross-sections and decay widths

Here, we collect all relevant reduced cross-sections  $\hat{\sigma}$ , required for computing the corresponding thermal rate  $\gamma^{\text{eq}}$  used in the Boltzmann equations. We here only consider CP-conserving tree-level processes, namely  $\gamma^{\text{eq}}(i \rightarrow f) = \gamma^{\text{eq}}(f \rightarrow i)$ , whereas one in general has  $\gamma^{\text{eq}}(i \rightarrow f) = \gamma^{\text{eq}}(\bar{f} \rightarrow \bar{i})$  according to CPT invariance.

- $R_{\bar{\psi}\psi} \phi \rightarrow \psi\bar{\psi}$

$$\hat{\sigma}(R_{\bar{\psi}\psi} \phi \rightarrow \psi\bar{\psi}) = 2s\lambda \left(1, \frac{m_R^2}{s}, \frac{m_\phi^2}{s}\right) \frac{2^4 y^{12} m_\psi^{\frac{5}{2}} m_R^5}{(s - m_R^2 - m_\phi^2)^5} \sqrt{\frac{s + m_R(m_R - 4m_\psi) - m_\phi^2}{2m_R}} F(v), \quad (\text{A1})$$

with

$$F(v) = \frac{v \exp(4v \arctan[v^{-1}])}{(1 - \exp(-2\pi v))(1 + v^2)^2}$$

and

$$v = \frac{y^2}{8\pi} \sqrt{\frac{2m_R m_\psi}{s + m_R^2 - 4m_R m_\psi - m_\phi^2}}.$$

Moreover, as the Yukawa interaction is always attractive among particles and antiparticles, one has

$$\hat{\sigma}(R_{\bar{\psi}\bar{\psi}}\phi \rightarrow \bar{\psi}\bar{\psi}) = \hat{\sigma}(R_{\psi\psi}\phi \rightarrow \psi\psi) = 2\hat{\sigma}(R_{\bar{\psi}\psi}\phi \rightarrow \bar{\psi}\psi). \quad (\text{A2})$$

The factor of 2 for  $R_{\bar{\psi}\psi}$  can be understood as follows. The symmetry factor for  $R_{\psi\psi}$  is  $\frac{1}{2}(2 \times 2)^2$ , where  $1/2$  comes from the identical outgoing particles (phase-space integral reduced by  $1/2$ ) and  $(2 \times 2)$  is owing to the different ways for the Yukawa interaction to annihilate the initial state and create the final state:  $\langle \psi\psi | \phi \bar{\psi}\psi | \phi\psi\psi \rangle$ . By contrast,  $R_{\bar{\psi}\psi}$  only has a symmetry factor of  $(2)^2$  coming from two ways of annihilating and creating the initial state and final state:  $\langle \bar{\psi}\bar{\psi} | \phi \bar{\psi}\psi | \phi\bar{\psi}\psi \rangle$ . As a consequence, there is a relative factor of 2 between the cases of  $R_{\psi\psi}$  and  $R_{\bar{\psi}\psi}$ .

- $R_{\bar{\psi}\psi} \rightarrow \phi\phi$

The decay width of  $R_{\bar{\psi}\psi}$  at rest can be obtained by adapting the results from Eq. (5.57) of Ref. [89], where the bound state decay is induced by the massless photon. With simply replacing  $\alpha_{em}^2$  with  $\frac{y^2}{4\pi}$ , we have:

$$\Gamma_{R_{\bar{\psi}\psi}} = \frac{4y^4}{79\pi} \frac{|\Psi_{100}(0)|^2}{m_R^2}, \quad (\text{A3})$$

where  $m_{R_{\bar{\psi}\psi}} = m_\psi \left(2 - \frac{y^4}{64\pi^2}\right)$  and  $\Psi_{100}(0)$  is the ground state wave function of  $R_{\bar{\psi}\psi}$  at  $r = 0$ . In the limit of  $m_\phi \sim 0 \ll m_\psi$ , the wave function reads

$$\Psi_{100}(0) = \frac{y^3 m_\psi^{3/2}}{16\sqrt{2}\pi^2}. \quad (\text{A4})$$

- $R_{\psi\psi} \rightarrow \chi\chi$  and  $R_{\bar{\psi}\bar{\psi}} \rightarrow \bar{\chi}\bar{\chi}$

The bound states  $R_{\psi\psi}$  and  $R_{\bar{\psi}\bar{\psi}}$  have the same decay width. In the limit of  $m_\psi \gg m_\chi$ ,

it reads

$$\Gamma_{R_{\psi\psi}} = \Gamma_{R_{\bar{\psi}\bar{\psi}}} = \frac{|\kappa_\chi \kappa_\psi|^2 |\Psi_{100}(0)|^2 m_R^2}{12 (m_{\phi'}^2 - m_R^2)^2 \pi}, \quad (\text{A5})$$

where  $\kappa_\psi$  and  $\kappa_\chi$  are the couplings of  $\psi$  and  $\chi$  to the mediator  $\phi'$  in Eq. (7), respectively, and  $\Psi_{100}(0)$  is given by Eq. (A4).

- $\psi\psi \leftrightarrow \phi\phi$

The reduced cross-section in the limit of  $m_\psi \gg m_\phi$  is given by

$$\hat{\sigma}(s) = \frac{y^4}{4\pi} \left( \operatorname{arctanh} \left[ \sqrt{1 - \frac{4m_\psi^2}{s}} \right] - \sqrt{1 - \frac{4m_\psi^2}{s}} \right) \mathcal{S}(\zeta), \quad (\text{A6})$$

with the Sommerfeld enhancement factor [33, 90]

$$\mathcal{S}(\zeta) = \frac{2\pi\zeta}{1 - \exp(-2\pi\zeta)},$$

and

$$\zeta = \frac{y^2}{4\pi} \frac{1}{\sqrt{1 - \frac{4m_\psi^2}{s}}}.$$

## Appendix B: Bound State Formation and Dissociation

In this Section, we discuss the cross-section computation of bound state dissociation (BSD) for the bound state  $R_{\psi\psi}$  by closely following the formalism described in Ref. [91]. The bound state formation (BSF) rate can be straightforwardly derived from that of BSD via  $\gamma^{\text{eq}}(\psi\psi \rightarrow R_{\psi\psi}\phi) = \gamma^{\text{eq}}(R_{\psi\psi}\phi \rightarrow \psi\psi)$ , while Eq. (A2) can be used to infer the BSD rates for the other bound states,  $R_{\bar{\psi}\psi}$  and  $R_{\bar{\psi}\bar{\psi}}$ .

To compute the amplitude of BSD, one needs to know the wave-function overlap between the initial and final states. Therefore, the bound state wave function in the presence of a Yukawa potential is required. In general, it does not have an analytic expression (see, e.g., Refs [92, 93]). To simplify the calculation, in the following we will focus on regions of the parameter space where the Yukawa potential can be well approximated by a Coulomb potential, of which the wave function is well-known.

## 1. Non relativistic Case

We start with the case of non-relativistic  $\psi$ . The Yukawa potential is given by

$$V(r) = -\frac{y^2}{4\pi} \frac{\exp(-m_\phi r)}{r} = -\frac{y^2}{4\pi} \frac{1}{r} \left[ 1 - m_\phi r + \mathcal{O}((m_\phi r)^2) \right], \quad (\text{B1})$$

where  $y$  is the Yukawa coupling and  $m_\phi$  is the mass of the scalar mediator  $\phi$ . In case the mediator mass is much smaller than the inverse of the Bohr radius  $a_0$  ( $= 8\pi/(y^2 m_\psi)$ ), the Yukawa potential will be dominated by the leading term since  $m_\phi r \sim m_\phi a_0 \ll 1$ , leading to a Coulomb potential. Under this approximation, we can solve the Schrödinger equation for the Coulomb potential and obtain the ground state wave function

$$\Psi_i(r) = \frac{m_\psi^{3/2} y^3}{16\sqrt{2}\pi^2} \exp\left(-\frac{m_\psi y^2}{8\pi} r\right), \quad (\text{B2})$$

where the subscript  $i$  refers to the initial state, as well as the binding energy

$$E_B = -\frac{m_\psi y^4}{64\pi^2} + \frac{m_\phi y^2}{4\pi}. \quad (\text{B3})$$

The differential cross-section for the process of  $R_{\psi\psi} + \phi \rightarrow \psi + \psi$  is given by

$$\frac{d\sigma}{d\Omega} = \frac{|V_{fi}|^2}{(2\pi)^2 \mu_\psi |\mathbf{p}|}, \quad (\text{B4})$$

where  $\mathbf{p} \equiv \mu_\psi (\mathbf{p}_{\psi,1}/m_\psi - \mathbf{p}_{\psi,2}/m_\psi)$  is the relative momentum between the two  $\psi$  particles. Conservation of energy requires  $|\mathbf{p}| = \sqrt{2\mu_\psi(E_B + E_\phi)}$  and the matrix element  $V_{fi}$  is defined as:

$$V_{fi} = y \sqrt{\frac{2\pi}{E_\phi}} \int \Psi_i^* \exp(ikr) \Psi_f \equiv y \sqrt{\frac{2\pi}{E_\phi}} M_{fi}, \quad (\text{B5})$$

where  $k$  is the momentum of the  $\phi$  particle. In contrast to the matrix element presented in Chapter 56 of [91], a Yukawa-type interaction,  $\mathcal{L} \supset y\phi\bar{\psi}\psi$ , is considered here instead of the Coulomb interaction mediated by the photon,  $\mathcal{L} \supset e\bar{\psi}\gamma_\mu\psi A^\mu$ . Since the computation assumes the unbound  $\psi$  to be non-relativistic it is sufficient to use the solution of the Schrödinger equation with a positive energy eigenvalue for describing the unbound final state  $\Psi_f$ :

$$\Psi_f = \frac{m_\psi y^2}{4\sqrt{2\pi}|\mathbf{p}|} \frac{\exp(-i|\mathbf{p}|r)}{\sqrt{v}[1 - \exp(2\pi v)]} {}_1F_1(1 + iv, 2, 2i|\mathbf{p}|r). \quad (\text{B6})$$

Here, we have  $v = y^2 m / (8\pi |\mathbf{p}|)$  and only the  $l = 0$  component is included due to the angular momentum conservation. Furthermore, we assume  $\exp(ikr) \approx 1$ , which is a good approximation as long as the assumption of the Coulomb potential is valid, i.e.,  $m_\phi \ll y^2 m_\psi / (8\pi)$ . From Eqs. (B2) and (B6), the integral in Eq. (B5) becomes

$$V_{fi} = -\frac{y^6 \sqrt{m_\psi}}{2\sqrt{2\pi} E_\phi^{\frac{5}{2}}} \sqrt{\frac{v}{1 - \exp(-2\pi v)}} \frac{\exp(2v \arctan[v^{-1}])}{1 + v^2}. \quad (\text{B7})$$

Note that we have made a replacement of  $r \rightarrow 2r$  in the wave functions  $\psi_i$  and  $\psi_f$  in the integral (B5), since  $dr$  is defined as the position relative to the center of mass of the bound state, whereas the relative position is used before in the bound state wave functions (B2) and (B6). Since we are dealing with a bound state consisting of two particles of equal mass, there is a factor of 2 difference between these two quantities.

Finally, by integrating Eq. (B4) over the solid angle and employing the conservation of the kinetic energy,  $E_\phi = \frac{|\mathbf{p}|^2}{2\mu} + \frac{my^2}{64\pi^2} = \frac{|\mathbf{p}|^2}{m_\psi} (1 + v^2)$ , the cross-section for the non-relativistic BSD is obtained:

$$\sigma = \frac{y^{12} m_\psi^{\frac{5}{2}} \sqrt{E_B + E_\phi}}{2\pi^3 E_\phi^5} \frac{v \exp(4v \arctan[v^{-1}])}{(1 - \exp(-2\pi v))(1 + v^2)^2}. \quad (\text{B8})$$

For BSD of  $R_{\bar{\psi}\psi}$ , one has to include an additional factor of 1/2 to Eq. (B8) according to Eq. (A2). Moreover, it is more convenient to rewrite the result in terms of the center-of-mass energy  $s$  in order to apply Eq. (4). In the rest frame of the bound state, the center of mass energy is  $s = m_R^2 + 2m_R E_\phi + m_\phi^2$ . Thus, the cross-section becomes:

$$\sigma(s) = \frac{2^4 y^{12} m_\psi^{\frac{5}{2}} m_R^5}{(s - m_R^2 - m_\phi^2)^5} \sqrt{\frac{s + m_R(m_R - 4m_\psi) - m_\phi^2}{2m_R}} \frac{v \exp(4v \arctan[v^{-1}])}{(1 - \exp(-2\pi v))(1 + v^2)^2}, \quad (\text{B9})$$

with

$$v = \frac{y^2 m_\psi}{8\pi |\mathbf{p}|} = \frac{y^2}{8\pi} \sqrt{\frac{2m_\psi m_R}{s + m_R(m_R - 4m_\psi) - m_\phi^2}}.$$

## 2. Relativistic Case

For the case of relativistic  $\psi$ , we follow Chapter 57 of Ref. [91], where results of the hydrogen atom have to be adapted for the Yukawa coupling as above. To calculate the matrix element  $M_{fi}$ , defined in Eq. (B5), the initial and final state wave functions are



required. The unbound, outgoing  $\psi$  is assumed to be highly relativistic. Therefore, the wave function is taken to be a plane wave:

$$\psi_f = \sqrt{\frac{1}{2E_\psi}} u_f \exp(i\mathbf{p}\mathbf{r}). \quad (\text{B10})$$

Since the initial state is also relativistic now, the first-order relativistic correction should be included:

$$\psi_i = \left(1 - \frac{i}{2\mu_\psi} \gamma^0 \vec{\gamma} \vec{\nabla}\right) \frac{u_i}{\sqrt{2\mu_\psi}} \psi_{nr}, \quad (\text{B11})$$

where the wave function is derived in Chapter 39 of Ref. [91] and  $\psi_{nr}$  is simply the ground state wave function in Eq. (B2). Substituting these equations into (B5) yields

$$M_{fi} = \frac{1}{2\sqrt{\mu E_\psi}} \int d^3x \bar{u}_f \left( \gamma^0 - \frac{i}{2\mu_\psi} \vec{\gamma} \vec{\nabla} \right) u_i \psi_{nr} e^{-i(\mathbf{p}-\mathbf{k})\mathbf{r}}, \quad (\text{B12})$$

that results in

$$|M_{fi}|^2 = \frac{y^{10} m_\psi^4}{256\pi^4 E_\psi (\mathbf{p}-\mathbf{k})^4} \bar{u}_f A u_i (\bar{u}_f A u_i)^\dagger, \quad (\text{B13})$$

with

$$A = \frac{\gamma^0}{(\mathbf{p}-\mathbf{k})^2} + \gamma \frac{\mathbf{k}-\mathbf{p}}{2\mu_\psi (\mathbf{k}-\mathbf{p})^2}. \quad (\text{B14})$$

Here  $\mathbf{k}$  corresponds to the momentum of  $\phi$  and  $\mathbf{p}$  stands for the momentum of the unbound  $\psi$  in the rest frame of the bound state before the collision. After summing over the final spins and averaging over the initial ones, we obtain

$$\frac{d\sigma}{d\Omega} = \frac{y^{12} m_\psi^5 |\mathbf{p}|}{256\pi^5 E_\phi (\mathbf{p}-\mathbf{k})^6} \left( \frac{E_\psi + m_\psi}{(\mathbf{p}-\mathbf{k})^2} + \frac{E_\psi}{m_\psi^2} - \frac{\mathbf{p}^2 - \mathbf{k}^2}{m_\psi (\mathbf{p}-\mathbf{k})^2} \right). \quad (\text{B15})$$

In contrast to the case of the hydrogen atom, neither of the two particles forming the bound state can be treated at rest in this system. We have to first calculate  $\mathbf{k}'$  and  $\mathbf{p}'$  in the center-of-mass system of the collision, and then perform a Lorentz boost back into the rest frame of the bound state afterwards. The procedures are lengthy but straightforward, and will not be shown here. Additionally, the integral over the solid angle  $d\Omega$  in eq. (B15) can only be computed numerically. The resulting cross-section is a function of the center-of-mass energy ( $s = m_R^2 + 2m_R E_\phi + m_\phi^2$ ), the mass of  $\psi$  and the Yukawa coupling.

### Appendix C: Freeze-in Constrain on the interaction rate of $\chi\chi \leftrightarrow \psi\psi$

As emphasized in Section I, we focus on the scenario of freeze-in decay, where the bound state starts to decay (via  $\psi\psi \rightarrow \chi\chi$ ) only during or after the density of the bound state caught up with that of the free  $\psi$ . On the other hand, the process  $\chi\chi \leftrightarrow \psi\psi$  also transfers asymmetry from  $\psi$  to  $\chi$  if it is efficient ( $\Gamma_{\psi\psi \leftrightarrow \chi\chi} > H$ ) for temperatures below the mass of  $\psi$ . As our main goal in this work is to demonstrate that BSF and the freeze-in decay can preserve and convert asymmetry to attain two-component ADM, we have to make sure the aforementioned process is not in equilibrium before the freeze-in decay. Here, we discuss how to satisfy the out-of-equilibrium constraint.

The reduced cross-section of the process  $\chi\chi \leftrightarrow \psi\psi$  is given by:

$$\hat{\sigma} = \frac{s^2 \sqrt{1 - \frac{4m_\psi^2}{s}}}{8\pi \left[ (s - m_{\phi'}^2)^2 + m_{\phi'}^2 \Gamma_{\phi'}^2 \right]}, \quad (\text{C1})$$

and the thermal rate can be found from

$$\gamma^{\text{eq}}(a_1 a_2 \leftrightarrow f_1 f_2) = \frac{T}{64\pi^4} \int_{s_{\min}}^{\infty} ds \sqrt{s} \hat{\sigma}(s) K_1\left(\frac{\sqrt{s}}{T}\right).$$

In case  $m_{\phi'} > 2m_\psi$  and a small decay width, the narrow width approximation can be applied to evaluate the integral and we have

$$\gamma^{\text{eq}} \approx \frac{\kappa_\chi^2 \kappa_\psi^2 m_{\phi'}^3 T \sqrt{m_{\phi'}^2 - 4m_\psi^2}}{2^9 \pi^5 \Gamma_{\phi'}} K_1\left(\frac{m_{\phi'}}{T}\right). \quad (\text{C2})$$

To determine whether or not the process is in equilibrium, we need to compute the ratio of its interaction rate to the Hubble expansion rate. It reads

$$\frac{\Gamma_{\psi\psi \leftrightarrow \chi\chi}}{H} \approx 3.6 \cdot 10^{-6} \frac{\kappa_\chi^2 \kappa_\psi^2 M_{\text{Pl}} m_{\phi'}^3 \sqrt{m_{\phi'}^2 - 4m_\psi^2} K_1\left(\frac{m_{\phi'}}{T}\right)}{m_\psi^2 T^3 \Gamma_{\phi'}}, \quad (\text{C3})$$

which is required to be less than one for the out-of-equilibrium condition at  $T \lesssim m_\psi$ . If the mediator  $\phi'$  only couples to  $\chi$  and  $\psi$ , then the decay width is simply

$$\Gamma_{\phi'} = \frac{m_{\phi'}}{8\pi} (\kappa_\chi^2 + \kappa_\psi^2). \quad (\text{C4})$$

In this case, although the interaction rate is suppressed by a small factor of  $\kappa_\chi^2 \kappa_\psi^2$ , it is at the same time enhanced by the small decay width proportional to  $\kappa_{\chi,\psi}^2$ . All in all, the

interaction rate is only suppressed by the square of the couplings  $\kappa_{\chi,\psi}$ . Note that the bound state decay width is also proportional  $\kappa_{\chi,\psi}^2$  and demanding the decay to happen before BBN imposes a lower bound on values of the couplings. In this case, the suppression of  $\kappa^2$  is not strong enough to keep the process  $\psi\psi \leftrightarrow \chi\chi$  out of equilibrium at  $T \lesssim m_\psi$ . One solution is to involve additional decay channels for  $\phi'$  that increase the total decay width and hence weaken the resonance enhancement. In this way, the interaction rate is suppressed by  $\kappa_\chi^2 \kappa_\psi^2$ , and with reasonably small values of the couplings (without perturbing BBN) the out-of-equilibrium condition can be fulfilled. Alternatively, one can simply make  $m_{\phi'} < 2m_\psi$  to prevent the resonance enhancement. For the benchmark points listed in Table. II, the second solution is utilized by taking  $m_{\phi'} = m_\psi$  and we have numerically confirmed that all the points satisfy the decoupling constraint.

- 
- [1] M. Tanabashi et al. Review of Particle Physics. Phys. Rev., D98(3):030001, 2018.
  - [2] N. Aghanim et al. Planck 2018 results. VI. Cosmological parameters. 2018, 1807.06209.
  - [3] Steen Hannestad and Georg Raffelt. Cosmological mass limits on neutrinos, axions, and other light particles. JCAP, 0404:008, 2004, hep-ph/0312154.
  - [4] Steen Hannestad, Alessandro Mirizzi, Georg G. Raffelt, and Yvonne Y. Y. Wong. Neutrino and axion hot dark matter bounds after WMAP-7. JCAP, 1008:001, 2010, 1004.0695.
  - [5] Howard Baer, Andrew D. Box, and Heaya Summy. Mainly axion cold dark matter in the minimal supergravity model. JHEP, 08:080, 2009, 0906.2595.
  - [6] Kyu Jung Bae, Howard Baer, and Eung Jin Chun. Mixed axion/neutralino dark matter in the SUSY DFSZ axion model. JCAP, 1312:028, 2013, 1309.5365.
  - [7] Ernest Ma. Verifiable radiative seesaw mechanism of neutrino mass and dark matter. Phys. Rev., D73:077301, 2006, hep-ph/0601225.
  - [8] Kathryn M. Zurek. Multi-Component Dark Matter. Phys. Rev., D79:115002, 2009, 0811.4429.
  - [9] Brian Batell. Dark Discrete Gauge Symmetries. Phys. Rev., D83:035006, 2011, 1007.0045.
  - [10] Hiroki Fukuoka, Daijiro Suematsu, and Takashi Toma. Signals of dark matter in a supersymmetric two dark matter model. JCAP, 1107:001, 2011, 1012.4007.
  - [11] Genevieve Belanger, Kristjan Kannike, Alexander Pukhov, and Martti Raidal. Impact of semi-annihilations on dark matter phenomenology - an example of  $Z_N$  symmetric scalar dark

- matter. JCAP, 1204:010, 2012, 1202.2962.
- [12] Mayumi Aoki, Michael Duerr, Jisuke Kubo, and Hiroshi Takano. Multi-Component Dark Matter Systems and Their Observation Prospects. Phys. Rev., D86:076015, 2012, 1207.3318.
  - [13] I. P. Ivanov and V. Keus.  $Z_p$  scalar dark matter from multi-Higgs-doublet models. Phys. Rev., D86:016004, 2012, 1203.3426.
  - [14] Diego Chialva, P. S. Bhupal Dev, and Anupam Mazumdar. Multiple dark matter scenarios from ubiquitous stringy throats. Phys. Rev., D87(6):063522, 2013, 1211.0250.
  - [15] Julian Heeck and He Zhang. Exotic Charges, Multicomponent Dark Matter and Light Sterile Neutrinos. JHEP, 05:164, 2013, 1211.0538.
  - [16] Kamakshya Prasad Modak, Debasish Majumdar, and Subhendu Rakshit. A Possible Explanation of Low Energy  $\gamma$ -ray Excess from Galactic Centre and Fermi Bubble by a Dark Matter Model with Two Real Scalars. JCAP, 1503:011, 2015, 1312.7488.
  - [17] Mayumi Aoki, Jisuke Kubo, and Hiroshi Takano. Two-loop radiative seesaw mechanism with multicomponent dark matter explaining the possible  $\gamma$  excess in the Higgs boson decay and at the Fermi LAT. Phys. Rev., D87(11):116001, 2013, 1302.3936.
  - [18] Chao-Qiang Geng, Da Huang, and Lu-Hsing Tsai. Imprint of multicomponent dark matter on AMS-02. Phys. Rev., D89(5):055021, 2014, 1312.0366.
  - [19] Yuji Kajiyama, Hiroshi Okada, and Takashi Toma. Multicomponent dark matter particles in a two-loop neutrino model. Phys. Rev., D88(1):015029, 2013, 1303.7356.
  - [20] Subhaditya Bhattacharya, Aleksandra Drozd, Bohdan Grzadkowski, and Jose Wudka. Two-Component Dark Matter. JHEP, 10:158, 2013, 1309.2986.
  - [21] Sonja Esch, Michael Klasen, and Carlos E. Yaguna. A minimal model for two-component dark matter. JHEP, 09:108, 2014, 1406.0617.
  - [22] G. Blanger, F. Boudjema, A. Pukhov, and A. Semenov. micrOMEGAs4.1: two dark matter candidates. Comput. Phys. Commun., 192:322–329, 2015, 1407.6129.
  - [23] Kaustubh Agashe, Yanou Cui, Lina Necib, and Jesse Thaler. (In)direct Detection of Boosted Dark Matter. JCAP, 1410(10):062, 2014, 1405.7370.
  - [24] Joshua Berger, Yanou Cui, and Yue Zhao. Detecting Boosted Dark Matter from the Sun with Large Volume Neutrino Detectors. JCAP, 1502(02):005, 2015, 1410.2246.
  - [25] Joachim Kopp, Jia Liu, and Xiao-Ping Wang. Boosted Dark Matter in IceCube and at the Galactic Center. JHEP, 04:105, 2015, 1503.02669.

- [26] Gian F. Giudice, Doojin Kim, Jong-Chul Park, and Seodong Shin. Inelastic Boosted Dark Matter at Direct Detection Experiments. Phys. Lett., B780:543–552, 2018, 1712.07126.
- [27] S. Nussinov. TECHNOCOSMOLOGY: COULD A TECHNIBARYON EXCESS PROVIDE A ‘NATURAL’ MISSING MASS CANDIDATE? Phys. Lett., 165B:55–58, 1985.
- [28] Kathryn M. Zurek. Asymmetric Dark Matter: Theories, Signatures, and Constraints. Phys. Rept., 537:91–121, 2014, 1308.0338.
- [29] Kalliopi Petraki and Raymond R. Volkas. Review of asymmetric dark matter. Int. J. Mod. Phys., A28:1330028, 2013, 1305.4939.
- [30] Adam Falkowski, Joshua T. Ruderman, and Tomer Volansky. Asymmetric Dark Matter from Leptogenesis. JHEP, 05:106, 2011, 1101.4936.
- [31] Adam Falkowski, Eric Kuflik, Noam Levi, and Tomer Volansky. Light Dark Matter from Leptogenesis. Phys. Rev., D99(1):015022, 2019, 1712.07652.
- [32] Mads T. Frandsen and Wei-Chih Huang. Large Higgs quartic coupling and (A)DM from extended Bosonic Technicolor. 12 2019, 1912.02203.
- [33] A. Sommerfeld. ber die beugung und bremsung der elektronen. Annalen der Physik, 403(3):257–330, 1931.
- [34] Andrei D. Sakharov. Interaction of an Electron and Positron in Pair Production. Zh. Eksp. Teor. Fiz., 18:631–635, 1948. [Usp. Fiz. Nauk161,no.5,29(1991)].
- [35] Junji Hisano, S. Matsumoto, and Mihoko M. Nojiri. Unitarity and higher order corrections in neutralino dark matter annihilation into two photons. Phys. Rev., D67:075014, 2003, hep-ph/0212022.
- [36] Junji Hisano, Shigeki Matsumoto, and Mihoko M. Nojiri. Explosive dark matter annihilation. Phys. Rev. Lett., 92:031303, 2004, hep-ph/0307216.
- [37] John Ellis, Feng Luo, and Keith A. Olive. Gluino Coannihilation Revisited. JHEP, 09:127, 2015, 1503.07142.
- [38] John Ellis, Jason L. Evans, Feng Luo, and Keith A. Olive. Scenarios for Gluino Coannihilation. JHEP, 02:071, 2016, 1510.03498.
- [39] Seyong Kim and M. Laine. Rapid thermal co-annihilation through bound states in QCD. JHEP, 07:143, 2016, 1602.08105.
- [40] Wai-Yee Keung, Ian Low, and Yue Zhang. Reappraisal of dark matter co-annihilating with a top or bottom partner. Phys. Rev., D96(1):015008, 2017, 1703.02977.

- [41] P. Binetruy, G. Girardi, and P. Salati. Constraints on a System of Two Neutral Fermions From Cosmology. Nucl. Phys., B237:285–306, 1984.
- [42] Kim Griest and David Seckel. Three exceptions in the calculation of relic abundances. Phys. Rev., D43:3191–3203, 1991.
- [43] Maxim Pospelov and Adam Ritz. Astrophysical Signatures of Secluded Dark Matter. Phys. Lett., B671:391–397, 2009, 0810.1502.
- [44] Andrzej Hryczuk, Roberto Iengo, and Piero Ullio. Relic densities including Sommerfeld enhancements in the MSSM. JHEP, 03:069, 2011, 1010.2172.
- [45] Andrzej Hryczuk. The Sommerfeld enhancement for scalar particles and application to sfermion co-annihilation regions. Phys. Lett., B699:271–275, 2011, 1102.4295.
- [46] M. Beneke, Charlotte Hellmann, and P. Ruiz-Femenia. Heavy neutralino relic abundance with Sommerfeld enhancements - a study of pMSSM scenarios. JHEP, 03:162, 2015, 1411.6930.
- [47] M. Beneke, C. Hellmann, and P. Ruiz-Femenia. Non-relativistic pair annihilation of nearly mass degenerate neutralinos and charginos III. Computation of the Sommerfeld enhancements. JHEP, 05:115, 2015, 1411.6924.
- [48] J. Harz, B. Herrmann, M. Klasen, K. Kovačik, and M. Meinecke. SUSY-QCD corrections to stop annihilation into electroweak final states including Coulomb enhancement effects. Phys. Rev., D91(3):034012, 2015, 1410.8063.
- [49] Benedict von Harling and Kalliopi Petraki. Bound-state formation for thermal relic dark matter and unitarity. JCAP, 1412:033, 2014, 1407.7874.
- [50] Kalliopi Petraki, Marieke Postma, and Michael Wiechers. Dark-matter bound states from Feynman diagrams. JHEP, 06:128, 2015, 1505.00109.
- [51] Marco Cirelli, Thomas Hambye, Paolo Panci, Filippo Sala, and Marco Taoso. Gamma ray tests of Minimal Dark Matter. JCAP, 1510(10):026, 2015, 1507.05519.
- [52] Lauren Pearce, Kalliopi Petraki, and Alexander Kusenko. Signals from dark atom formation in halos. Phys. Rev., D91:083532, 2015, 1502.01755.
- [53] Haipeng An, Mark B. Wise, and Yue Zhang. Strong CMB Constraint On P-Wave Annihilating Dark Matter. Phys. Lett., B773:121–124, 2017, 1606.02305.
- [54] Kalliopi Petraki, Marieke Postma, and Jordy de Vries. Radiative bound-state-formation cross-sections for dark matter interacting via a Yukawa potential. JHEP, 04:077, 2017, 1611.01394.
- [55] Chris Kouvaris, Kasper Langble, and Niklas Grnlund Nielsen. The Spectrum of Darkonium

- in the Sun. JCAP, 1610:012, 2016, 1607.00374.
- [56] Sonia El Hedri, Anna Kaminska, and Maikel de Vries. A Sommerfeld Toolbox for Colored Dark Sectors. Eur. Phys. J., C77(9):622, 2017, 1612.02825.
  - [57] Seng Pei Liew and Feng Luo. Effects of QCD bound states on dark matter relic abundance. JHEP, 02:091, 2017, 1611.08133.
  - [58] Pouya Asadi, Matthew Baumgart, Patrick J. Fitzpatrick, Emmett Krupczak, and Tracy R. Slatyer. Capture and Decay of Electroweak WIMPonium. JCAP, 1702(02):005, 2017, 1610.07617.
  - [59] Haipeng An, Mark B. Wise, and Yue Zhang. Effects of Bound States on Dark Matter Annihilation. Phys. Rev., D93(11):115020, 2016, 1604.01776.
  - [60] Marco Cirelli, Paolo Panci, Kalliopi Petraki, Filippo Sala, and Marco Taoso. Dark Matter’s secret liaisons: phenomenology of a dark U(1) sector with bound states. JCAP, 1705(05):036, 2017, 1612.07295.
  - [61] Seyong Kim and M. Laine. On thermal corrections to near-threshold annihilation. JCAP, 1701:013, 2017, 1609.00474.
  - [62] S. Biondini and M. Laine. Re-derived overclosure bound for the inert doublet model. JHEP, 08:047, 2017, 1706.01894.
  - [63] Iason Baldes, Marco Cirelli, Paolo Panci, Kalliopi Petraki, Filippo Sala, and Marco Taoso. Asymmetric dark matter: residual annihilations and self-interactions. SciPost Phys., 4(6):041, 2018, 1712.07489.
  - [64] Iason Baldes and Kalliopi Petraki. Asymmetric thermal-relic dark matter: Sommerfeld-enhanced freeze-out, annihilation signals and unitarity bounds. JCAP, 1709(09):028, 2017, 1703.00478.
  - [65] S. Biondini and M. Laine. Thermal dark matter co-annihilating with a strongly interacting scalar. JHEP, 04:072, 2018, 1801.05821.
  - [66] S. Biondini. Bound-state effects for dark matter with Higgs-like mediators. JHEP, 06:104, 2018, 1805.00353.
  - [67] S. Biondini and Stefan Vogl. Coloured coannihilations: Dark matter phenomenology meets non-relativistic EFTs. JHEP, 02:016, 2019, 1811.02581.
  - [68] John Ellis, Jason L. Evans, Feng Luo, Keith A. Olive, and Jiaming Zheng. Stop Coannihilation in the CMSSM and SubGUT Models. Eur. Phys. J., C78(5):425, 2018, 1801.09855.

- [69] Michael Geller, Sho Iwamoto, Gabriel Lee, Yael Shadmi, and Ofri Telem. Dark quarkonium formation in the early universe. JHEP, 06:135, 2018, 1802.07720.
- [70] Julia Harz and Kalliopi Petraki. Radiative bound-state formation in unbroken perturbative non-Abelian theories and implications for dark matter. JHEP, 07:096, 2018, 1805.01200.
- [71] Marco Cirelli, Yann Gouttenoire, Kalliopi Petraki, and Filippo Sala. Homeopathic Dark Matter, or how diluted heavy substances produce high energy cosmic rays. JCAP, 1902:014, 2019, 1811.03608.
- [72] Arindam Bhattacharya and Tracy R. Slatyer. Bound States of Pseudo-Dirac Dark Matter. JCAP, 1903(03):029, 2019, 1812.03169.
- [73] S. Schmiemann, J. Harz, B. Herrmann, M. Klasen, and K. Kovarik. Squark-pair annihilation into quarks at next-to-leading order. Phys. Rev., D99(9):095015, 2019, 1903.10998.
- [74] Julia Harz and Kalliopi Petraki. Higgs Enhancement for the Dark Matter Relic Density. Phys. Rev., D97(7):075041, 2018, 1711.03552.
- [75] Julia Harz and Kalliopi Petraki. Higgs-mediated bound states in dark-matter models. JHEP, 04:130, 2019, 1901.10030.
- [76] Tobias Binder, Kyohei Mukaida, and Kalliopi Petraki. Rapid bound-state formation of Dark Matter in the Early Universe. 2019, 1910.11288.
- [77] John McDonald. Thermally generated gauge singlet scalars as selfinteracting dark matter. Phys. Rev. Lett., 88:091304, 2002, hep-ph/0106249.
- [78] Lawrence J. Hall, Karsten Jedamzik, John March-Russell, and Stephen M. West. Freeze-In Production of FIMP Dark Matter. JHEP, 03:080, 2010, 0911.1120.
- [79] Nicols Bernal, Matti Heikinheimo, Tommi Tenkanen, Kimmo Tuominen, and Ville Vaskonen. The Dawn of FIMP Dark Matter: A Review of Models and Constraints. Int. J. Mod. Phys., A32(27):1730023, 2017, 1706.07442.
- [80] Joakim Edsjo and Paolo Gondolo. Neutralino relic density including coannihilations. Phys. Rev., D56:1879–1894, 1997, hep-ph/9704361.
- [81] G. F. Giudice, A. Notari, M. Raidal, A. Riotto, and A. Strumia. Towards a complete theory of thermal leptogenesis in the SM and MSSM. Nucl. Phys., B685:89–149, 2004, hep-ph/0310123.
- [82] Motohiko Yoshimura. Unified Gauge Theories and the Baryon Number of the Universe. Phys. Rev. Lett., 41:281–284, 1978. [Erratum: Phys. Rev. Lett. 42,746(1979)].
- [83] D. Toussaint, S. B. Treiman, Frank Wilczek, and A. Zee. Matter - Antimatter Accounting,



- Thermodynamics, and Black Hole Radiation. Phys. Rev., D19:1036–1045, 1979.
- [84] Steven Weinberg. Cosmological Production of Baryons. Phys. Rev. Lett., 42:850–853, 1979.
  - [85] Stephen M. Barr, Gino Segre, and H. Arthur Weldon. The Magnitude of the Cosmological Baryon Asymmetry. Phys. Rev., D20:2494, 1979.
  - [86] Celine Boehm, Matthew J. Dolan, and Christopher McCabe. Increasing  $N_{\text{eff}}$  with particles in thermal equilibrium with neutrinos. JCAP, 1212:027, 2012, 1207.0497.
  - [87] Kenneth M. Nollett and Gary Steigman. BBN And The CMB Constrain Neutrino Coupled Light WIMPs. Phys. Rev., D91(8):083505, 2015, 1411.6005.
  - [88] Marco Hufnagel, Kai Schmidt-Hoberg, and Sebastian Wild. BBN constraints on MeV-scale dark sectors. Part I. Sterile decays. JCAP, 1802:044, 2018, 1712.03972.
  - [89] Michael E. Peskin and Daniel V. Schroeder. An Introduction to quantum field theory. 1995.
  - [90] Marco Cirelli, Alessandro Strumia, and Matteo Tamburini. Cosmology and Astrophysics of Minimal Dark Matter. Nucl. Phys., B787:152–175, 2007, 0706.4071.
  - [91] E.M. Lifhsitz V.B. Berestetskii and L.P. Pitaevskii. Quantum Electrodynamics. USA: Addison-Wesley 842 p, 1982.
  - [92] M. Hamzavi, M. Movahedi, K.-E. Thylwe, and A. A. Rajabi. Approximate analytical solution of the yukawa potential with arbitrary angular momenta. Chinese Physics Letters, 29(8):080302, aug 2012.
  - [93] F. J. Rogers, H. C. Graboske, and D. J. Harwood. Bound eigenstates of the static screened coulomb potential. Phys. Rev. A, 1:1577–1586, Jun 1970.